nature materials

ARTICLES

https://doi.org/10.1038/s41563-020-0774-9

Check for updates

Intrinsic quantum confinement in formamidinium lead triiodide perovskite

Adam D. Wright[1], George Volonakis[2,3], Juliane Borchert[1], Christopher L. Davies[1], Feliciano Giustino[2,4,5], Michael B. Johnston[1] and Laura M. Herz[1]✉

Understanding the electronic energy landscape in metal halide perovskites is essential for further improvements in their promising performance in thin-film photovoltaics. Here, we uncover the presence of above-bandgap oscillatory features in the absorption spectra of formamidinium lead triiodide thin films. We attribute these discrete features to intrinsically occurring quantum confinement effects, for which the related energies change with temperature according to the inverse square of the intrinsic lattice parameter, and with peak index in a quadratic manner. By determining the threshold film thickness at which the amplitude of the peaks is appreciably decreased, and through ab initio simulations of the absorption features, we estimate the length scale of confinement to be 10–20 nm. Such absorption peaks present a new and intriguing quantum electronic phenomenon in a nominally bulk semiconductor, offering intrinsic nanoscale optoelectronic properties without necessitating cumbersome additional processing steps.

Metal halide perovskites are renowned for their spectacular performance as photovoltaic active layers[1,2], with single-junction perovskite solar cells now achieving power conversion efficiencies (PCEs) of over 25% (ref. [3]). This success stems from their excellent material properties, such as high charge-carrier mobilities, low exciton binding energies, broad absorption across the solar spectrum[1,4] and facile fabrication routes[5]. Although perovskite solar cells typically incorporate thin films of three-dimensional (3D, bulk) perovskite, nanostructures have also been engineered not only for solar cells, but also light-emitting diodes, lasers and photodetectors[6]. Whether nanocrystals (0D), nanowires (1D) or nanoplates (2D) are employed, the reduced dimensionality results in quantum confinement of charge carriers that yields dramatically different optoelectronic properties, including enhanced photoluminescence quantum yield[7] and lower thresholds for amplified spontaneous emission[8].

Although the creation of such perovskite nanostructures has clear advantages, it often relies on challenging top-down fabrication methods[6,9]. It would therefore be highly beneficial if instead nanoscale domains were found to form intrinsically through self-assembly in the perovskite. Intrinsic domains have in fact already been observed[10–14] in films of methylammonium lead triiodide ($MAPbI_3 = CH_3NH_3PbI_3$). However, although these polar domains may be associated with electronic barriers[15–17], their reported widths range between 90 and 300 nm (refs. [11–13]), roughly an order of magnitude too large to result in appreciable quantum confinement effects[6,9]. Intriguingly, there have been some recent suggestions that these domains are ferroelectric[13,14], although others have instead considered them to arise from ferroelastic effects[12,18]. The presence of mobile ions has also been found to mimic ferroelectric signatures[12], making this a contentious topic.

Formamidinium lead triiodide ($FAPbI_3 = CH(NH_2)_2PbI_3$) may be a far more promising candidate than $MAPbI_3$ for displaying intrinsic quantum confinement. The proposed presence of twin domains bounded by the non-perovskite δ-phase of $FAPbI_3$ (refs. [19,20]) could, for example, lead to the formation of intrinsic nanostructures. In addition, as detailed in Supplementary Note 13, the combination of the greater polar deformation and smaller dipole–dipole interaction energy attributable to the FA cation[21] gives reason[22] to expect any polar ferroelectric domains in $FAPbI_3$ to be smaller than in $MAPbI_3$ and hence engender more substantial quantum confinement. Compared with $MAPbI_3$, $FAPbI_3$ is more resistant to heat stress[23] and has a narrower bandgap that is closer to optimal for solar cells[23–25]. It furthermore exhibits good charge-carrier mobility[26], long charge-carrier diffusion length[26] and impressive PCEs in solar cells[27]. We thus examine $FAPbI_3$ as a promising material for displaying intrinsic quantum confinement, despite it being investigated to a far lesser extent than $MAPbI_3$.

In this work, we report the discovery of intrinsically occurring nanostructures in $FAPbI_3$ that exhibit quantum confinement effects manifested as an oscillatory absorption feature above the bandgap. These features are present at room temperature but sharpen and become more apparent as the temperature is lowered towards 4 K. We demonstrate that the energetic spacings and temperature dependence of the peaks vary in a manner consistent with quantum confinement intrinsically associated with the lattice of the material. We suggest that the origin of this confinement is nanodomains with an extent of approximately 10–20 nm. This interpretation is supported by correlating absorption spectra with ab initio calculations based on the band structure of $FAPbI_3$ in the presence of infinite barriers, and with simulations of superlattices with moderate barrier heights. We further explore ferroelectricity and/or ferroelasticity and δ-phase twin boundaries as two possible causes of these domains. Altogether, such oscillatory absorption of $FAPbI_3$ presents an intriguing intrinsic quantum electronic phenomenon in a highly promising semiconducting material.

Fig. 1a reveals oscillatory features in the absorption spectrum of $FAPbI_3$ films that are just discernible at room temperature but

[1]Clarendon Laboratory, Department of Physics, University of Oxford, Oxford, UK. [2]Department of Materials, University of Oxford, Oxford, UK. [3]Univ Rennes, ENSCR, INSA Rennes, CNRS, ISCR (Institut des Sciences Chimiques de Rennes) - UMR 6226, Rennes, France. [4]Oden Institute for Computational Engineering and Sciences, The University of Texas at Austin, Austin, TX, USA. [5]Department of Physics, The University of Texas at Austin, Austin, TX, USA. ✉e-mail: laura.herz@physics.ox.ac.uk

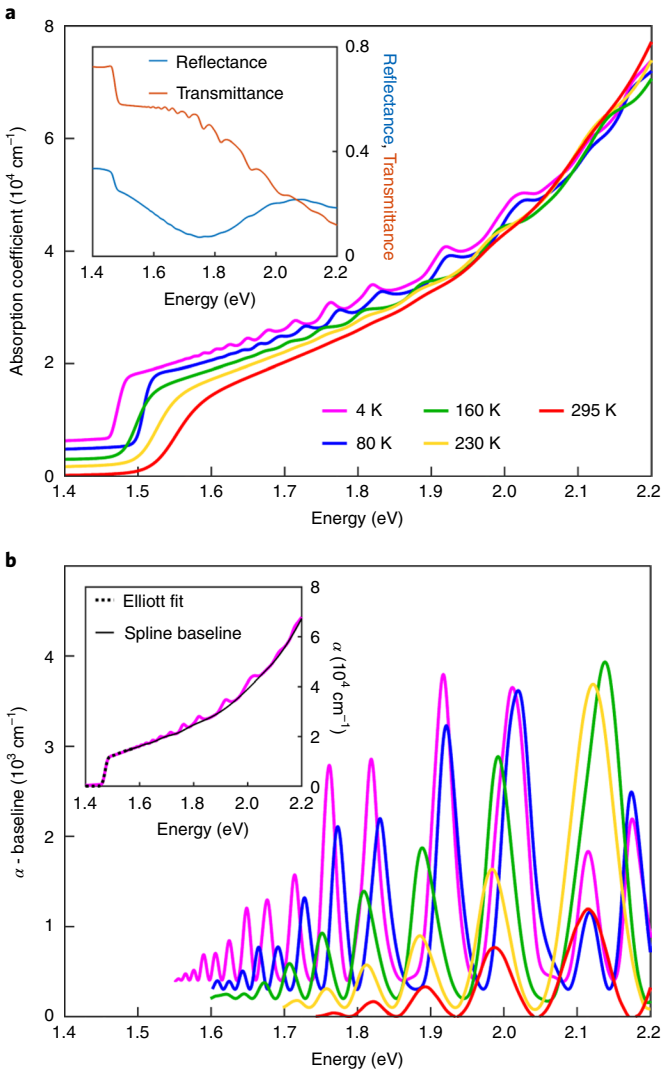

Fig. 1 | Temperature-dependent absorption coefficient and peak features. **a**,**b**, Absorption spectra (**a**) and peaks (**b**) for a 297-nm-thick $FAPbI_3$ film measured by FTIR spectroscopy at roughly 70 K temperature intervals from 4 K to 295 K (the legend in **a** also applies to **b**). Spectra for further temperatures and film thicknesses are shown in Supplementary Figure 5. For clarity, spectra and peaks at successively decreasing temperatures are offset vertically by 1.5×10^3 cm^{-1} and 1×10^2 cm^{-1} respectively. The inset in **a** depicts the reflectance and transmittance of the film at 4 K. The inset in **b** shows the absorption coefficient (α) at 4 K with its absorption onset fitted by a function based on Elliott's theory (dotted black line) and the oscillatory region fitted with a spline baseline fit (solid black line), which is subtracted from the absorption coefficient to give the peaks shown in **b**.

become much more prominent towards lower temperatures. $FAPbI_3$ thin films were fabricated by dual-source vapour deposition, as detailed in Supplementary Note 1, which produces highly uniform and smooth thin films[28] exhibiting minimal scattering effects and sharp absorption onsets, as evident from Fig. 1a. Both reflection and transmission measurements (see inset) were taken from 4 K up to 295 K using a Fourier-transform infrared (FTIR) spectrometer, and the absorption coefficient was obtained as detailed in Supplementary Note 3. We took great care to ensure that the observed oscillatory features did not result from optical interference (Fabry–Pérot oscillations), were not specific to the measurement technique and did not conflict with what is known of $FAPbI_3$ thin-film absorption (see Supplementary Note 3). We further proved that they were specific to the semiconducting perovskite phases of $FAPbI_3$ thin films alone (they were absent in its yellow δ-phase) and did not appear in a $MAPbI_3$ thin film measured under identical conditions (Supplementary Note 3).

Fig. 1a demonstrates that for $FAPbI_3$, the typically smoothly rising absorption onset of a semiconductor is modulated with additional peak features. To allow better visualization and quantification of the oscillatory peaks, we therefore decouple them from the underlying absorption spectrum, albeit only phenomenologically. As shown in the inset to Fig. 1b, we fitted a spline baseline to the above-bandgap absorption data using the procedure detailed in Supplementary Note 4. Subtracting this baseline from the absorption spectrum yielded only the peak features, whose temperature dependence is shown in Fig. 1b for a 297-nm-thick $FAPbI_3$ film, and for other film thicknesses in Supplementary Fig. 10. In isolation from the overall absorption spectra, the peaks can be clearly seen to increase in both amplitude and energy spacing with increasing energy, and to reduce in amplitude with temperature.

We further find that the energies of the peak maxima display subtle shifts with temperature (Fig. 1b). However, such shifts may also derive from modifications to the bandgap energy E_g of the semiconductor, rather than changes in quantization energy with temperature. To decouple such effects, we therefore determine E_g by modelling the onsets of the measured $FAPbI_3$ absorption spectra with fits based on Elliott's theory (Supplementary Note 4 and Supplementary Figs. 9 and 11), which describes the absorption spectra of semiconductors as arising from both bound excitons and electron–hole continuum states[29], and has been successfully applied to metal halide perovskites[25,30,31]. The resultant values of E_g (Fig. 2a) and the exciton binding energy (Supplementary Fig. 12) for the six films ranging in thickness from 35 nm to 840 nm, are consistent with previous reports[24,25,32,33] and with photoluminescence measurements (Supplementary Note 5). We note that E_g decreases slightly with increasing film thickness, possibly due to the increased lattice strain present in thinner films [9].

From the positions of the peak energies (E_{peak}) relative to E_g (Fig. 2c) we are able to demonstrate through multiple pieces of evidence that quantum confinement effects cause the observed absorption features. First, comparison between the temperature dependencies of E_g (Fig. 2a) and $E_g - E_{peak}$ (Fig. 2c) clearly proves that the peaks are influenced by temperature independently of the bandgap and mostly also of film thickness (see also Supplementary Note 6 and Supplementary Fig. 14). In fact, the peaks generally shift in the opposite direction from E_g with temperature, with a small interruption by the transition from the γ-phase to the β-phase near 140 K. These trends can be fully understood if they are considered to arise from changes in the lattice parameter of $FAPbI_3$, which lead to a concomitant reduction of the intrinsic domains or substructure from which the quantum confinement derives. To examine such correlations, we considered the temperature dependence of the reduced lattice parameters, p (ref. [35]) ($p = a/\sqrt{2}, c$ for the β-phase, $p = a/\sqrt{2}, c/6$ for the γ-phase, where a and c are the width and height, respectively, of the tetragonal unit cell) of $FAPbI_3$, taken from a previous neutron diffraction report[34]. As discussed in more detail below, if the peaks observed in the absorption spectra arise from the presence of intrinsic electronic barriers, for example, in the form of a quasi-infinite potential well or a superlattice, then the confinement energy $E_{peak} - E_g$ will depend on the inverse square of the well width or superlattice period (see Supplementary Note 7). As these lengths scale with p, any changes in the associated confinement energies must be proportional to $1/p^2$. Figure 2f reveals that $1/p^2$ has a very similar dependence on temperature to $E_{peak} - E_g$ for both sets of reduced lattice parameters on either side of the β–γ phase transition. To indicate this similarity more quantitatively, the inset in Fig. 2f shows the ratio Q of the temperature gradients of $1/p^2$ and $E_{peak} - E_g$ (for peak series 12 of the 297-nm-thick film; see

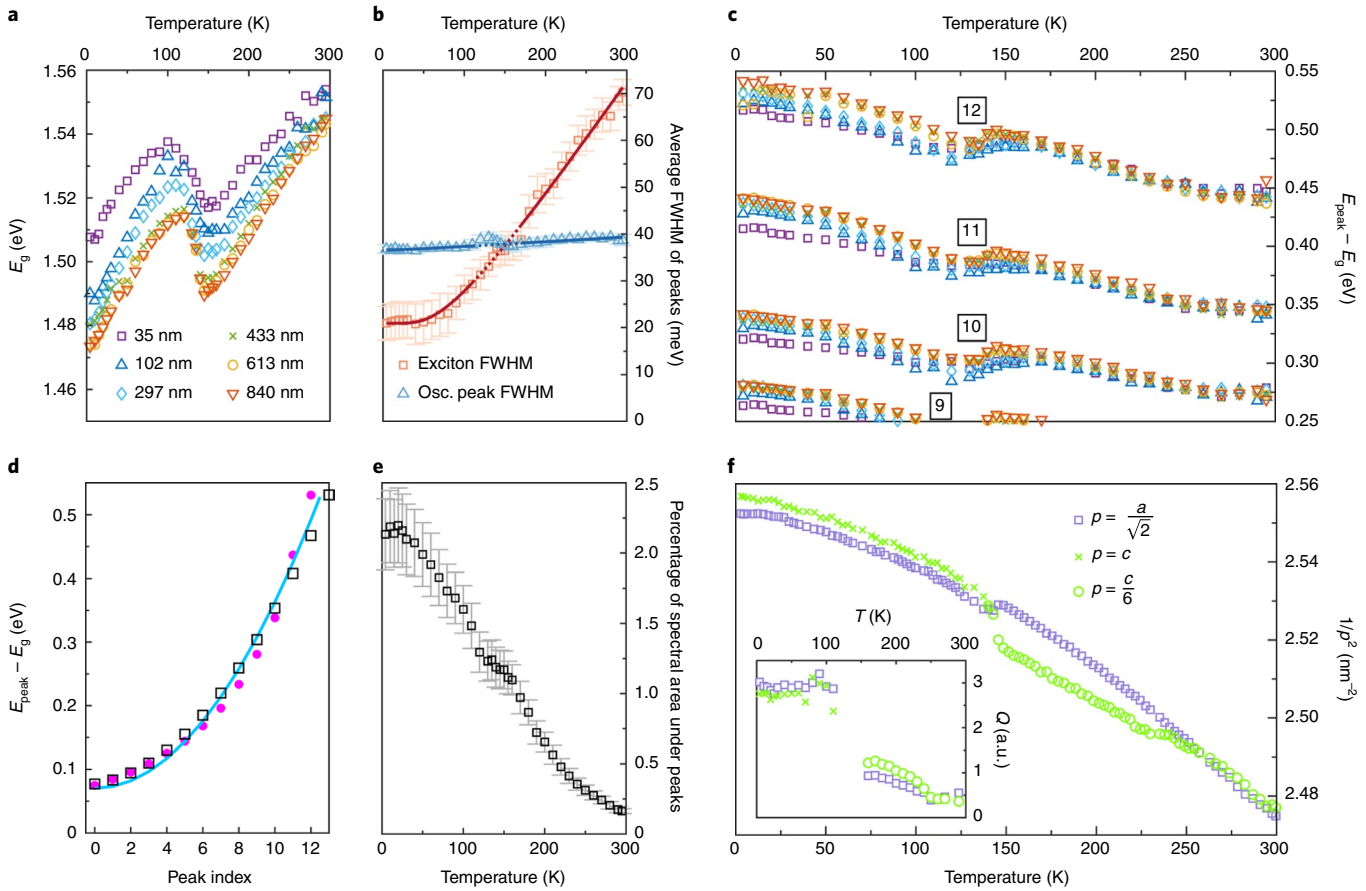

Fig. 2 | Temperature dependence of the optoelectronic and lattice properties of $FAPbI_3$. **a**, E_g extracted from Elliott fits to the absorption spectra for films of six thicknesses (see the legend). **b**, Linewidth (full-width at half-maximum, FHWM) of the excitonic peak extracted from the Elliott fits (red squares) and the most prominent peaks (blue triangles), averaged across the six film thicknesses. The dark solid lines are fits that account for Fröhlich coupling with LO phonons, excluding temperatures near the phase transition (dotted lines). Error bars show the standard error. **c**, E_{peak} relative to E_g. Boxed numbers show the peak indices. **d**, Variation of $E_{peak} - E_g$ (magenta dots) at 4 K in the 297-nm-thick film as a function of the peak index. The solid blue line is a fit based on a quadratic function whereas the black squares represent E_g values derived from a Krönig–Penney potential (see Supplementary Note 7). The offset of the lowest-energy peaks from E_g may be attributed to a slightly higher bandgap within the nanostructures, shifted by ~70 meV due to lattice strain within the nanostructure[9,23]. **e**, Integral (area) under the main peaks (black squares) as a percentage of the total area under the spectrum, averaged across the six thicknesses. Error bars show the standard error. **f**, Temperature dependence of $1/p^2$ for p defined in the legend. The inset shows Q, which is given by the ratio of the temperature gradients in $E_{peak} - E_g$ to those in $1/p^2$ for the 297-nm-thick film (see Supplementary Note 8). Panel **f** adapted with permission from ref. [34], American Chemical Society.

Supplementary Note 8 for details). Away from the phase transition, Q seems relatively temperature independent, suggesting that the changes in $E_{peak} - E_g$ are largely derived from modifications in the extent of the intrinsic domains in $FAPbI_3$ that give rise to the quantum confinement.

Second, our assignment of these peaks to electronic confinement is also supported by the quadratic relationship between peak index n and $E_{peak} - E_g$, displayed in Fig. 2d. To illustrate this point, we examine two confinement potential scenarios, represented by either the simple 'particle in a box' model of an infinite quantum well, or a superlattice comprising a periodic arrangement of quantum wells separated by semipermeable barriers (see Supplementary Note 7 for full details). Both models accurately predict the above-bandgap energy to scale with n^2, as observed, because the associated **k** vector scales with the inverse of the quantum well width, or superlattice period, respectively. However, as we show in Supplementary Notes 7 and 10, for the case of the superlattice represented by a Krönig–Penney potential, more moderate (finite) potential barriers can still give rise to peak features at energies exceeding E_g by more than the potential height. We suggest such superlattices may derive from clusters containing nanostructures of similar extent, with our calculated band energies expected for a superlattice (plotted as black squares in Fig. 2d) agreeing well with our observed peak positions. These arguments therefore confirm that peaks may arise from electronic barriers present in the material in the form of quantum wells or coupled superlattices.

As a third point, we note that the peaks are broadened in a fundamentally different manner from the bulk states associated with the excitonic peak near the onset of absorption. Figure 2b compares the temperature-dependent broadening of the peaks (plotted in blue) with the broadening of the bulk excitonic states (plotted in red), showing distinct magnitudes and trends. By assuming such temperature-dependent broadening to arise from electronic coupling to longitudinal optical (LO) phonons (see Supplementary Note 6), we determine an LO phonon energy $E_{LO} = 19$ meV and coupling strength $\gamma_{LO} = 57$ meV for the broadening associated with the excitonic absorption onset, broadly consistent with previous reports for this material[24,36]. In contrast, the corresponding fit to the linewidths of the additional peak features (solid blue line in Fig. 2b) yields substantially lower values of only 0.7 meV and 6 meV, respectively,

indicating a considerably different origin of the broadening. As an explanation, we note that a reduction in coupling strength to optical phonons is symptomatic of semiconductors with reduced dimensionality[37,38], again pointing towards quantum confinement as the cause of the peaks.

If quantum confinement is intrinsic to semiconducting $FAPbI_3$, one way to explore its origin is to consider the effective length scale of the structure to which charge carriers are confined. We tackle this challenge with a two-pronged approach, first by examining the dependence of the peaks on film thickness, and second through ab initio calculations aimed at reproducing the observed features from calculations based on the $FAPbI_3$ band structure under confinement. Our experimental approach reveals that the positions of the peaks have little dependence on the $FAPbI_3$ film thickness between 35 nm and 840 nm (see Supplementary Fig. 10 and derived data in Fig. 2c). This observation proves that the film surfaces themselves do not provide the boundaries of electronic confinement, as we would otherwise expect the energy of confinement to scale roughly inversely with the square of the film thickness. A different, intrinsic length scale of quantum confinement may therefore be involved, and is likely to be considerably smaller than the film thickness. To explore the magnitude of this intrinsic scale, we reduced the nominal film thickness further, below 35 nm to the point at which the peaks had appreciably weakened in amplitude. We note that down to a thickness of 35 nm, the strength of the absorption peaks observed had also been relatively independent of film thickness (see Supplementary Fig. 10). However, as indicated in Fig. 3a, once the film thickness is further lowered to 10 nm, the amplitude of the peaks at 4 K has decreased by at least a factor of four compared with the 35-nm-thick film sample, and peaks are no longer visible at room temperature (Supplementary Fig. 22). The tenuous presence of absorption peaks in the 10-nm-thick film suggests that its thickness is close to the minimum at which this phenomenon can occur, and is hence similar to the length scale of confinement, with local ordering disrupted for film thicknesses that undercut this intrinsic domain size.

We further examine the length scale of confinement through density functional theory (DFT)[39–41] calculations that simulate the effects of quantum confinement on the absorption spectra of $FAPbI_3$, here for the simple case of infinite potential barriers in all three dimensions. Full details of these calculations can be found in Supplementary Note 9. Figure 3b shows the resultant absorption coefficient spectra, calculated using confinement lengths (L_{DFT}) ranging from 3 nm to 17 nm. As expected, these calculated spectra exhibit peaks corresponding to the energy transitions between quantized valence and conduction band states, which become more closely spaced with increasing L_{DFT}. For comparison, we also display the experimentally measured absorption spectrum for the 297-nm-thick film at 4 K (black line), which indicates that the best correspondence between the peak features in the measured and calculated spectra occurs for $L_{DFT} = 13$ nm or 17 nm. We therefore note that taking into account both experimental variation of film thickness and ab initio calculations indicates that quantum confinement occurs on a length scale of 10–20 nm, which is feasible given our 10–15 nm estimate of the excitonic Bohr radius in $FAPbI_3$ in Supplementary Note 14.

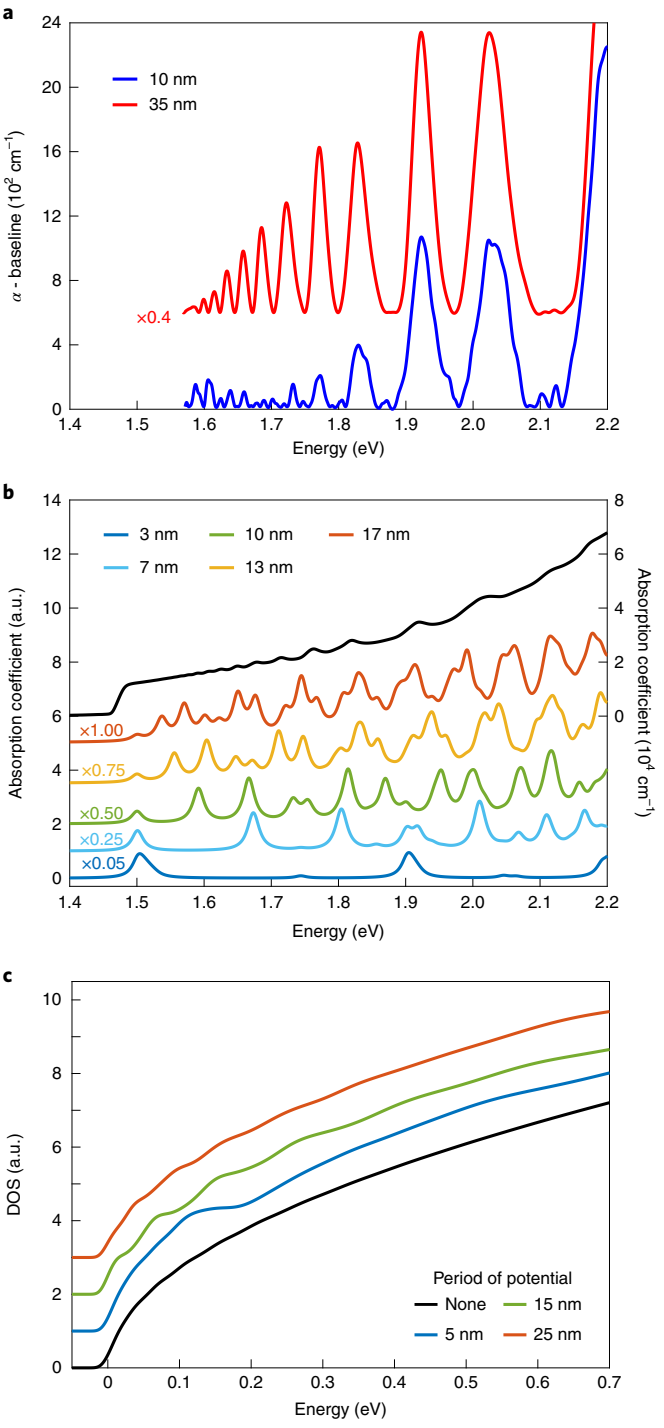

Fig. 3 | Estimating the length scale of the structures inducing confinement. a, Measured absorption peaks of 10-nm-thick and 35-nm-thick (offset vertically by 6×10^2 cm^{-1} and scaled vertically by a factor of 0.4) films of $FAPbI_3$ at 4 K. **b**, Measured and calculated absorption coefficient of $FAPbI_3$. The measured spectrum (black line), taken at 4 K for the 297-nm-thick film, uses the vertical scale on the right. The calculated spectra are vertically offset from each other and scaled vertically by the factors indicated in the corresponding colours. They are based on a simple particle-in-a-box system with confinement in three dimensions, taking the actual band structure of $FAPbI_3$ into account using first-principles calculations. A spectral broadening of 10 meV is used for these calculated spectra, which are simulated at 0 K (see Supplementary Note 9) and use the vertical scale on the left. **c**, Calculated density of states (DOS) for a one-dimensional superlattice for the periods indicated. Calculations are based on a model using a Krönig–Penney potential, assuming a square-like periodic wave potential, with wall width b here set to one-tenth of the period $a + b$ (see Supplementary Note 10 for full details). Here, the DOS is shown for a fixed potential amplitude of 250 meV, but with variations in superlattice period $a + b$. The black line shows the free-electron case (with no periodic potential), representing a square-root function.

We note at this point, however, that we cannot definitively ascertain the number of dimensions the electronic system is confined in, as our baseline removal procedure may remove any underlying, continuous density of states that may also be associated with the quantum confinement. Whereas electronic confinement by infinite potential wells in all three directions (as in our first-principles approach; see Fig. 3b) directly yields peak-like absorption features similar to the features we isolate through the baseline approach, one-dimensional confinement gives rise to additional continuum states associated with free motion in the other two dimensions, which may however be removed by our baselines fits to also produce peak-like features (see Supplementary Notes 4 and 10). Similarly, as Fig. 3c indicates, a 1D superlattice displays absorption features modulating an otherwise relatively smooth underlying density of states (see Supplementary Note 10 for full calculations based on a model using a Krönig–Penney potential). Although we thus cannot determine the dimensionality of confinement, or the fraction of the material that exhibits confinement, we find these to be consistent across different film thicknesses, probably because such dual-source vapour deposition has previously been found to result in highly uniform morphology[42] independent of film thickness. We further note that the sharpness of the peak features modulating the $FAPbI_3$ absorption spectra indicates the disorder attributable to any variation in the length scales of confinement to be relatively low.

Having uncovered the presence of quantum confinement in $FAPbI_3$, we need to identify the origin of such potential wells. We propose two possible causes of intrinsic confinement in $FAPbI_3$: the presence of δ-phase barriers, and the formation of nanoscale ferroelectric or ferroelastic domains. Our discussion accounts for the various trends observed, including the clear weakening of the features with increasing temperature (Fig. 2e). Moreover, the mild (70 meV) energetic offset of the first peaks from the bandgap (see Supplementary Note 7 and the quadratic fit in Fig. 2d) could indicate that lattice strain is prominent in the confinement regions[9,23]. Furthermore, a device based on a similar film (shown in Supplementary Note 2) achieves a short-circuit current density of 80% of the theoretical maximum, suggesting a low presence of impermeable barriers to charge motion; the performance of this device is compatible with the presence of an intrinsic electronic superlattice structure.

We first examine the possibility that small inclusions of non-perovskite δ-phase could act as potential barriers within an otherwise semiconducting perovskite $FAPbI_3$. The δ-phase of $FAPbI_3$ is yellow and so has a substantially wider bandgap than the perovskite phases, making it in principle suitable as a potential barrier material. In support of this argument, we note that $FAPbI_3$ films that were originally in the perovskite α-phase at room temperature have been found in some cases (using neutron diffraction) to contain δ-phase on cooling[43], although not in other measurements[34]. The absence[44] of an equivalent δ-phase in $MAPbI_3$ would further explain why we find similar peaks to be absent in its absorption spectra. Although DFT calculations have predicted that {111} twin boundaries (which structurally correspond to the δ-phase) in $FAPbI_3$ are associated with an electronic barrier height of less than 100 meV (ref. [20]), a periodic superlattice with such low potential barriers corresponding to δ-phase twin boundaries could still cause absorption peaks at higher energies, as shown in Supplementary Notes 7 and 10. We find that prominent features arise from such structures even for thin barriers of less than 10% of the width of the potential wells between them, which could still be compatible with the apparent absence of a visible δ-phase peak in the X-ray diffraction patterns of our $FAPbI_3$ films within their detection limit (see Supplementary Fig. 1). In addition, we note that although the absorption peaks seem to disappear above a temperature of ~380 K (Supplementary Fig. 23), which is near the temperature at which the δ-phase transitions to the α-phase[34], these features can reappear when the sample is cooled again. Whereas α-phase is usually metastable at room temperature for an extended period[34], it is possible that strained regions may respond with the spontaneous formation of δ-phase superlattices on cooling.

An alternative possibility is that the absorption peaks arise from quantum confinement within ferroelectric or ferroelastic domains in $FAPbI_3$. As detailed above, such domains had not been observed in $FAPbI_3$, but have been examined in more detail in $MAPbI_3$, for which they have been proposed to be between 90 and 300 nm wide[12,13]. On the basis of comparisons of the dielectric properties for the two materials (see Supplementary Note 13), we would estimate polar domains in $FAPbI_3$ to be approximately twenty times smaller, in good agreement with the length scales of 10–20 nm on which we find charge carriers to be quantum confined. Ferroelectric domain walls in $PbTiO_3$ (ref. [45]) and $BiFeO_3$ (ref. [46]) have been calculated to present potential steps of up to 180 meV, which is again a feasible height for a periodic superlattice potential to cause absorption features such as those we observe. However, ferroelectricity has been extensively debated for $MAPbI_3$, for which some authors[12,47] consider this phenomenon to be impossible at room temperature. Our data are not necessarily in contention with this claim, given that we observe a temperature-dependent decline in the amplitude of the peaks (Fig. 2e) that is similar in shape to that observed for the spontaneous polarisation of a ferroelectric material with a second-order phase transition[48]. In addition, the reappearance of the peaks when cooling down from 380 K mirrors the spontaneous reappearance of polarization in ferroelectrics below their Curie temperature[13]. Such behaviour is also a feature of ferroelasticity, the phenomenon that has been proposed as an alternative cause of the domains observed in $MAPbI_3$ (refs. [12,18]). Thus we believe that quantum confinement may arise from either ferroelectric or ferroelastic domains in $FAPbI_3$.

In summary, we have discovered peak features in the absorption spectra of $FAPbI_3$ arising from discrete optical transitions of electrons between quantum confined states and potentially caused by the formation of ferroelastic or polar ferroelectric domains, or δ-phase inclusions. Our analysis is supported by relative peak energies with respect to the band edge scaling with temperature according the inverse square of the intrinsic lattice parameter, and with peak index in a quadratic fashion. By observing a threshold film thickness of 10 nm at which the amplitude of peaks is appreciably decreased, and through ab initio simulations of the absorption features, we estimate the length scale of quantum confinement to be 10–20 nm. These observations represent an exciting discovery because they offer the highly sought-after goal of electronic quantum confinement without the requirement of extensive top-down nanoprocessing steps, while maintaining efficient flow of electrical current. Such nanostructures offer the narrowed-down densities of states required to enhance radiative emission, lower thresholds for amplified spontaneous emission and facilitate electrical injection lasing.

Online content

Any methods, additional references, Nature Research reporting summaries, source data, extended data, supplementary information, acknowledgements, peer review information; details of author contributions and competing interests; and statements of data and code availability are available at https://doi.org/10.1038/s41563-020-0774-9.

Received: 1 April 2020; Accepted: 16 July 2020;
Published online: 24 August 2020

References

1. Johnston, M. B. & Herz, L. M. Hybrid perovskites for photovoltaics: charge-carrier recombination, diffusion, and radiative efficiencies. *Acc. Chem. Res.* **49**, 146–154 (2016).
2. Kojima, A., Teshima, K., Shirai, Y. & Miyasaka, T. Organometal halide perovskites as visible-light sensitizers for photovoltaic cells. *J. Am. Chem. Soc.* **131**, 6050–6051 (2009).

3. *NREL Research Cell Record Efficiency Chart* (NREL, 2019).
4. Herz, L. M. Charge-carrier dynamics in organic-inorganic metal halide perovskites. *Annu. Rev. Phys. Chem.* **67**, 65–89 (2016).
5. Stoumpos, C. C. & Kanatzidis, M. G. Halide perovskites: poor man's high-performance semiconductors. *Adv. Mater.* **28**, 5778–5793 (2016).
6. Fu, Y. et al. Metal halide perovskite nanostructures for optoelectronic applications and the study of physical properties. *Nat. Rev. Mater.* **4**, 169–188 (2019).
7. Polavarapu, L., Nickel, B., Feldmann, J. & Urban, A. S. Advances in quantum-confined perovskite nanocrystals for optoelectronics. *Adv. Energy Mater.* **7**, 1–9 (2017).
8. Li, M. et al. Amplified spontaneous emission based on 2D Ruddlesden–Popper perovskites. *Adv. Funct. Mater.* **28**, 1707006 (2018).
9. Parrott, E. S. et al. Growth modes and quantum confinement in ultrathin vapour-deposited $MAPbI_3$ films. *Nanoscale* **11**, 14276–14284 (2019).
10. Hermes, I. M. et al. Ferroelastic fingerprints in methylammonium lead iodide perovskite. *J. Phys. Chem. C* **120**, 5724–5731 (2016).
11. Rothmann, M. U. et al. Direct observation of intrinsic twin domains in tetragonal $CH_3NH_3PbI_3$. *Nat. Commun.* **8**, 6–13 (2017).
12. Wilson, J. N., Frost, J. M., Wallace, S. K. & Walsh, A. Dielectric and ferroic properties of metal halide perovskites. *APL Mater.* **7**, 010901 (2019).
13. Röhm, H. et al. Ferroelectric properties of perovskite thin films and their implications for solar energy conversion. *Adv. Mater.* **31**, 1806661 (2019).
14. Röhm, H., Leonhard, T., Hoffmann, M. J. & Colsmann, A. Ferroelectric poling of methylammonium lead iodide thin films. *Adv. Funct. Mater.* **30**, 1908657 (2020).
15. Liu, S. et al. Ferroelectric domain wall induced band gap reduction and charge separation in organometal halide perovskites. *J. Phys. Chem. Lett.* **6**, 693–699 (2015).
16. Montero-Alejo, A. L., Menéndez-Proupin, E., Palacios, P., Wahnón, P. & Conesa, J. C. Ferroelectric domains may lead to two-dimensional confinement of holes, but not of electrons, in $CH_3NH_3PbI_3$ perovskite. *J. Phys. Chem. C* **121**, 26698–26705 (2017).
17. Pecchia, A., Gentilini, D., Rossi, D., Auf der Maur, M. & Di Carlo, A. Role of ferroelectric nanodomains in the transport properties of perovskite solar cells. *Nano Lett.* **16**, 988–992 (2016).
18. Gómez, A., Wang, Q., Goñi, A. R., Campoy-Quiles, M. & Abate, A. Reply to the "Comment on the publication 'Ferroelectricity-free lead halide perovskites' by Gomez et al." by Colsmann et al. *Energy Environ. Sci.* **13**, 1892–1895 (2020).
19. Weller, M. T., Weber, O. J., Frost, J. M. & Walsh, A. Cubic perovskite structure of black formamidinium lead iodide, α-$[HC(NH_2)_2]PbI_3$, at 298 K. *J. Phys. Chem. Lett.* **6**, 3209–3212 (2015).
20. McKenna, K. P. Electronic properties of {111} twin boundaries in a mixed-ion lead halide perovskite solar absorber. *ACS Energy Lett.* **3**, 2663–2668 (2018).
21. Frost, J. J. M. J. et al. Atomistic origins of high-performance in hybrid halide perovskite solar cells. *Nano Lett.* **14**, 2584–2590 (2014).
22. Lines, M. E. & Glass, A. M. *Principles and Applications of Ferroelectrics and Related Materials* (Oxford Univ. Press, 1977).
23. Eperon, G. E. et al. Formamidinium lead trihalide: a broadly tunable perovskite for efficient planar heterojunction solar cells. *Energy Environ. Sci.* **7**, 982–988 (2014).
24. Wright, A. D. et al. Electron-phonon coupling in hybrid lead halide perovskites. *Nat. Commun.* **7**, 11755 (2016).
25. Davies, C. L. et al. Impact of the organic cation on the optoelectronic properties of formamidinium lead triiodide. *J. Phys. Chem. Lett.* **9**, 4502–4511 (2018).
26. Rehman, W. et al. Charge-carrier dynamics and mobilities in formamidinium lead mixed-halide perovskites. *Adv. Mater.* **27**, 7938–7944 (2015).
27. Li, Y. et al. Formamidinium-based lead halide perovskites: structure, properties, and fabrication methodologies. *Small Methods* **2**, 1700387 (2018).
28. Borchert, J. et al. Large-area, highly uniform evaporated formamidinium lead triiodide thin films for solar cells. *ACS Energy Lett.* **2**, 2799–2804 (2017).
29. Elliott, R. J. Intensity of optical absorption by excitons. *Phys. Rev.* **108**, 1384–1389 (1957).
30. Davies, C. et al. Bimolecular recombination in methylammonium lead triiodide perovskite is an inverse absorption process. *Nat. Commun.* **9**, 293 (2018).
31. Sestu, N. et al. Absorption F-sum rule for the exciton binding energy in methylammonium lead halide perovskites. *J. Phys. Chem. Lett.* **6**, 4566–4572 (2015).
32. Francisco-López, A. et al. Phase diagram of methylammonium/formamidinium lead iodide perovskite solid solutions from temperature-dependent photoluminescence and raman spectroscopies. *J. Phys. Chem. C* **124**, 3448–3458 (2020).
33. Wright, A. D. et al. Band-tail recombination in hybrid lead iodide perovskite. *Adv. Funct. Mater.* **27**, 1700860 (2017).
34. Weber, O. J. et al. Phase behavior and polymorphism of formamidinium lead iodide. *Chem. Mater.* **30**, 3768–3778 (2018).
35. Brivio, F. et al. Lattice dynamics and vibrational spectra of the orthorhombic, tetragonal and cubic phases of methylammonium lead iodide. *Phys. Rev. B* **92**, 144308 (2015).
36. Fang, H.-H. et al. Photoexcitation dynamics in solution-processed formamidinium lead iodide perovskite thin films for solar cell applications. *Light Sci. Appl* **5**, e16056 (2016).
37. Bockelmann, U. & Bastard, G. Phonon scattering and energy relaxation in two-, one-, and zero-dimensional electron gases. *Phys. Rev. B* **42**, 8947–8951 (1990).
38. Alivisatos, A. P., Harris, T. D., Carroll, P. J., Steigerwald, M. L. & Brus, L. E. Electron-vibration coupling in semiconductor clusters studied by resonance Raman spectroscopy. *J. Chem. Phys.* **90**, 3463–3468 (1989).
39. Marini, A., Hogan, C., Grüning, M. & Varsano, D.yambo: an ab initio tool for excited state calculations. *Comp. Phys. Commun.* **180**, 1392–1403 (2009).
40. Giannozzi, P. et al. QUANTUM ESPRESSO: a modular and open-source software project for quantum simulations of materials. *J. Phys. Condens. Matter* **21**, 395502 (2009).
41. Perdew, J. P., Burke, K. & Ernzerhof, M. Generalized gradient approximation made simple. *Phys. Rev. Lett.* **77**, 3865–3868 (1996).
42. Crothers, T. W. et al. Photon re-absorption masks intrinsic bimolecular charge-carrier recombination in $CH_3NH_3PbI_3$ rerovskite. *Nano Lett.* **17**, 5782–5789 (2017).
43. Chen, T. et al. Entropy-driven structural transition and kinetic trapping in formamidinium lead iodide perovskite. *Sci. Adv.* **2**, e1601650 (2016).
44. Stoumpos, C., Malliakas, C. & Kanatzidis, M. Semiconducting tin and lead iodide perovskites with organic cations: phase transitions, high mobilities, and near-infrared photoluminescent properties. *Inorg. Chem.* **52**, 9019–9038 (2013).
45. Meyer, B. & Vanderbilt, D. Ab initio study of ferroelectric domain walls in $PbTiO_3$. *Phys. Rev. B* **65**, 104111 (2002).
46. Seidel, J. et al. Conduction at domain walls in oxide multiferroics. *Nat. Mater.* **8**, 229–234 (2009).
47. Gómez, A., Wang, Q., Goñi, A. R., Campoy-Quiles, M. & Abate, A. Ferroelectricity-free lead halide perovskites. *Energy Environ. Sci.* **12**, 2537–2547 (2019).
48. Martin, L. W. & Rappe, A. M. Thin-film ferroelectric materials and their applications. *Nat. Rev. Mater.* **2**, 16087 (2016).

Methods

Sample preparation. $FAPbI_3$ thin films were grown on *z*-cut quartz substrates using a dual-source thermal evaporation system (Kurt J. Lesker) as reported previously[25,28]. The precursors were FAI purchased from Greatcell Solar Materials and PbI_2 from Alfa Aesar. These precursors were placed in separate alumina crucibles and heated until they evaporated. The samples were mounted on a rotating substrate holder to enable uniform deposition. The deposited films were annealed at 170° C for 1 min to ensure that they were in the desired perovskite phase of $FAPbI_3$.

Device fabrication. A solar cell based on an evaporated $FAPbI_3$ film was fabricated using a standard architecture. The substrate was fluoride-doped tin oxide (FTO) coated glass, onto which the fullerene C_{60} from Acros Organics was evaporated at 350 °C. The perovskite layer was co-evaporated onto this as described above. Next the hole extraction material 2,2′,7,7′-Tetrakis-(*N*,*N*-di-4-methoxyphenylamino)-9,9′-spirobifluorene (Spiro-OMeTAD) from Lumtec was spin coated on top. Spiro-OMeTAD was doped with lithium bis(trifluoromethanesulfonyl)imide (LiTFSI) and 4-*tert*-Butylpyridine (tBP) and the solution spin coated at 2,000 r.p.m. for 45 s. Finally, 100 nm of silver was evaporated to contact the solar cells. The size of the evaporated metal contacts was 0.0919 cm^2.

X-ray diffraction. X-ray diffraction patterns of $FAPbI_3$ films were measured in air using a Panalytical X'pert powder diffractometer with a copper X-ray source.

Current–voltage measurements. Current–voltage measurements were carried out on the solar cell device (based on an evaporated $FAPbI_3$ film) under illumination with an ABET class AAB sun 2000 simulator. The scan speed was 0.38 V s^{-1}.

Reflection–transmission measurements. To measure the temperature-dependent reflectance and transmittance of $FAPbI_3$ films, a Bruker Vertex 80 v FTIR spectrometer was used, configured with a tungsten halogen lamp illumination source, a CaF_2 beamsplitter and a silicon detector. The samples were mounted in a gas-exchange helium cryostat (Oxford Instruments, OptistatCF2) and heated over a temperature range of 4 to 295 K in increments of between 5 and 10 K.

Photoluminesence measurements. To measure the temperature-dependent photoluminescence of $FAPbI_3$ films, the sample was photoexcited by a 398 nm picosecond pulsed diode laser (PicoHarp, LDH-D-C-405M). The resultant photoluminescence was collected and coupled into a grating spectrometer (Princeton Instruments, SP-2558), which directed the spectrally dispersed photoluminescence onto a silicon iCCD (PI-MAX4, Princeton Instruments). The sample was mounted under vacuum ($P < 10^{-6}$ mbar) in a cold-finger liquid helium cryostat (Oxford Instruments, MicrostatHe) and heated over a temperature range of 4 to 295 K in increments of between 3 and 6 K.

First-principles calculations. The electronic band structure of $FAPbI_3$ at 0 K was simulated using a simplified, abstract cubic lattice structure that lacks the FA cation. This method avoided the complexities of the FA cation orientation while ensuring that E_g and the band dispersion were consistent with experimentally measured values[49]. Next, the effect of electronic confinement was introduced to this band structure by generating a discrete *k*-point grid of the wavevectors allowed for a particle confined by infinite barriers in all three dimensions within a confinement length L_{DFT}. The absorption coefficient arising from such confined electronic states was then computed as resulting from transitions between the conduction band and valence band states lying on the *k*-point grid of our simulated band structure.

Data availability

The datasets generated during and/or analysed during the current study are available in the Oxford University Research Archive repository[50].

References

49. Chen, T. et al. Origin of long lifetime of band-edge charge carriers in organic-inorganic lead iodide perovskites. *Proc. Natl Acad. Sci. USA* **114**, 7519–7524 (2017).
50. Wright, A. D. et al. Dataset for 'Intrinsic quantum confinement in formamidinium lead triiodide perovskite'. *Oxford University Research Archive* https://doi.org/10.5287/bodleian:Z52M67emQ (2020).

Acknowledgements

This work was supported by the Engineering and Physical Sciences Research Council, the EPSRC Center for Doctoral Training in New and Sustainable Photovoltaics, the Chaire de Recherche Rennes Metropole project and the Robert A. Welch Foundation under award number F-1990-20190330.

Author contributions

A.D.W. performed the FTIR experiments, data analysis and participated in the experimental planning. G.V. carried out the first-principles calculations. J.B. prepared the samples. C.L.D. provided support with the FTIR experiments and data analysis. The project was conceived, planned and supervised by F.G., M.B.J. and L.M.H. A.D.W. wrote the first version of the manuscript and all authors contributed to the discussion and preparation of the final version of the article.

Competing interests

The authors declare no competing interests.

Additional information

Supplementary information is available for this paper at https://doi.org/10.1038/s41563-020-0774-9.

Correspondence and requests for materials should be addressed to L.M.H.

Reprints and permissions information is available at www.nature.com/reprints.